through the isosbestic point, and we propose that the reaction represented by eq 1 may also be important for solutions with low concentrations of free NCS^- (where X = NCS^- and Y = acetone or impurities in the solvent, such as water). This postulate is consistent with the fact that the solution with the lowest concentration of $[Cu(TIM)NCS]PF_6$ in the Onsager study gives an equivalent conductance higher than that predicted from the straight line described by the other four points.

The picture for the $Cu(TIM)^{2+}$–Cl^- system is considerably less well developed than that for the NCS^- system just described. A deliquescent solid, tentatively formulated as $Cu(TIM)Cl_2$, forms from a blue oil, which in turn separates from acetone solutions of $Cu(TIM)(PF_6)\cdot xH_2O$ and excess LiCl. The solid is soluble in CH_2Cl_2 and $CHCl_3$. In the latter the molecular weight is found to be 440 (calculated for $[Cu(TIM)Cl_2]$, 383) with benzil as a standard. Given that this experimental value is 15% high and that for the NCS^- derivative is 16% high, it would seem that the two complexes exhibit similar states of aggregation in $CHCl_3$.

Specifying the exact nature of the copper–axial ligand interaction for some complexes of the Cu(TIM) class clearly is not trivial and must be approached with great care whether in the solid phase or in solution.

Acknowledgment. We wish to thank A. Reuveni for his help in obtaining and interpreting the EPR spectra and Professor R. A. Palmer for obtaining the photoacoustic spectrum of $[Cu(TIM)](BPh_4)_2$. M.J.M. gratefully acknowledges fellowships sponsored by Georgia-Pacific Corp. and Chevron Research Co. in support of this research.

Contribution from the Department of Chemistry, University of Washington, Seattle, Washington 98195

Electronic Structure of Copper Complexes Containing α-Diimine Ligands[1]

MICHAEL J. MARONEY,* JOE G. NORMAN, JR., and JOSEPH H. OSBORNE

Received January 31, 1983

SCF–Xα–SW calculations have been carried out for $Cu(N_2C_2H_4)_2^{2+}$ and $Cu(N_2C_2H_4)_2Cl^+$, the simplest possible models for planar $Cu(TIM)^{2+}$ and pyramidal $Cu(TIM)Cl^+$, respectively, where TIM is a 14-membered macrocycle containing two α-diimine moieties. The electronic and EPR spectra of the complexes are interpreted with use of the results of the calculations. The electronic absorptions observed for $[Cu(TIM)][BPh_4]_2$ at 2.94 and 3.85 μm^{-1} are confidently assigned to the LMCT transitions. The lowest energy absorptions observed for $[Cu(TIM)][BPh_4]_2$ and $[Cu(TIM)Cl][PF_6]$ are best described as intermediate in character between LMCT and d–d transitions. The largest factor influencing the energy of the lowest energy transition is shown to be the degree of copper atom displacement from the basal ligand plane. The effects of adding a fifth ligand to the planar complex to produce a pyramidal complex are discussed. Little covalency is predicted to result from the interaction of the Cu(II) and apical Cl^- centers in $Cu(TIM)Cl^+$. The covalent bonding that is present appears to be almost entirely σ in character. The role of Cu 4s and 4p orbitals in the bonding scheme of $Cu(TIM)Cl^+$ is predicted to be small. The ground state calculated for the reduced complex, $Cu(TIM)^+$, contains a Cu(I) center obtained by addition of the electron acquired upon reduction to a molecular orbital that is largely Cu d_{xy} in character. The intense absorption experimentally observed in the electronic spectrum of $Cu(TIM)^+$ is assigned to a $d_{xy} \rightarrow \pi^*$ MLCT transition. No significant π interaction between Cu and ligand π* orbitals is predicted to occur in the ground state of $Cu(TIM)^+$, but a significant fraction of the electron added upon reduction does end up in the ligand σ-electron systems. This may explain the lowering of $\nu_{C=N}$ that has been observed upon reduction of Cu(II) α-diimine complexes.

Introduction

Complexes of the neutral, 14-membered, macrocyclic ligand TIM (**1**) have been synthesized and characterized for first-row

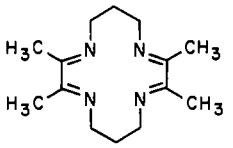

1

transition-metal ions of Fe,[2-5] Co,[6,7] Ni,[8] and Cu.[9] In many cases the ligand possesses the ability to stabilize more than one oxidation state of a metal and is capable of allowing for facile interconversion of two oxidation states.[4] Four-,[10] five-,[10,11] and six-coordinate[2-5,8,12] complexes of TIM have been characterized via single-crystal X-ray diffraction techniques, and TIM invariably features a planar arrangement of its four N-donor atoms.

The coordination chemistry of copper complexes of TIM, discussed in the preceding paper, is extremely varied. Four-, five-, and six-coordinate complexes have been characterized in the solid state,[9-12] and five- and six-coordinate complexes have been characterized in solution.[9] Copper is the only metal explored to date that displays all three possible coordination numbers with TIM.

Both Cu(II) and formally Cu(I) complexes have been prepared.[9] The latter have been characterized only in solutions that are not stable in air. The electronic structure of formally

* To whom correspondence should be addressed at the Department of Chemistry, University of Minnesota, Minneapolis, MN 55455.

(1) Presented in part at the 36th Northwest Regional Meeting of the American Chemical Society, Bozeman, MT, June 1981; see Abstract No. INOR 93.
(2) Baldwin, D. A.; Pfeiffer, R. M.; Reichgott, D. W.; Rose, N. J. *J. Am. Chem. Soc.* **1973**, *95*, 5152–5158.
(3) Reichgott, D. W. Ph.D. Thesis, University of Washington, 1976.
(4) Reichgott, D. W.; Rose, N. J. *J. Am. Chem. Soc.* **1977**, *99*, 1813–1818.
(5) Fey, E. O. Ph.D. Thesis, University of Washington, 1979.
(6) Farmery, K.; Kildahl, N. K.; Busch, D. H. *J. Coord. Chem.* **1980**, *10*, 85–100.
(7) Jackels, S. C.; Farmery, K.; Barefield, E. K.; Rose, N. J.; Busch, D. H. *Inorg. Chem.* **1972**, *11*, 2893–2901.
(8) Baldwin, D. A.; Rose, N. J. "Abstracts of Papers", 157th National Meeting of the American Chemical Society, Minneapolis, MN, April 1969; American Chemical Society: Washington, DC, 1969; INOR 020.
(9) Maroney, M. J.; Rose, N. J. *Inorg. Chem.*, preceding paper in this issue.
(10) Elia, A. Ph.D. Thesis, University of Washington, 1982.
(11) Elia, A.; Santarsiero, B. D.; Lingafelter, E. C.; Schomaker, V. *Acta Crystallogr., Sect. B: Cryst. Chem.* **1982**, *B38*, 3020–3023.
(12) Pajunen, A. *Acta Crystallogr., Sect. B: Struct. Crystallogr. Cryst. Chem.* **1982**, *B38*, 928–929.

0020-1669/84/1323-2261$01.50/0

Cu(I) complexes of tetraimine macrocycles has been the topic of considerable debate in the recent literature.[13-17] Much of the controversy centers on attempting to describe the four-coordinate complexes in terms of oxidation-state formalisms for the copper centers. The three oxidation-state formalisms that seem plausible are $[Cu^{I}(N_4)]^+$, $[Cu^{II}(N_4^-)]^+$, and $[Cu^{III}(N_4^{2-})]^+$, where N_4 represents a tetraimine macrocyclic ligand. The second and third models depend upon the reduction of the ligand in preference to the metal center, a process which is well documented in the chemistry of synthetic macrocycles containing conjugated imines.[16,18] The third model also represents an intramolecular electron rearrangement consisting of the transfer of an electron from Cu to the ligand in addition to the one-electron reduction of the macrocycle. Intramolecular electron transfers have been demonstrated for Co(TAAB)[16] and for $Ni(LBF_2)^+$ and related macrocycles.[18] The latter study demonstrated the effects of geometry and macrocycle ring size on the electron rearrangement. Both the reduction of the ligand in preference to the metal and facile intramolecular electron rearrangements for these macrocycles are dependent upon ligand π^* levels lying close in energy to the metal d_{xy} orbital. With use of EPR, it was shown that reduction of planar $[Ni^{II}(N_4^-)]^+$ leads to a complex best described as $[Ni^{II}(N_4^{2-})]$ and that factors having stabilizing effects on the Ni d_{xy} orbital (i.e., the displacement of the metal from the N_4 plane by the addition of a fifth ligand[18] and an increase in the flexibility of the macrocycle and Ni–N bonds[18,19]) result in complexes described as containing Ni(I) centers.

Conclusions as to the electronic structure of planar Cu complexes of TIM, LBF_2, and TAAB have been drawn on the basis of both experiments and theory. The electronic structure of $Cu(TAAB)^+$ has been described in terms of the oxidation-state formalism $[Cu^{III}(N_4^{2-})]^+$, in analogy to the known chemistry of $Ni(TAAB)^+$ and $Co(TAAB)^+$. From EPR and electrochemical studies,[15,16] these last complexes have been described as containing Ni(II), Co(II), and the aromatic dianion $TAAB^{2-}$. The results of X-ray photoelectron spectroscopic studies on $Cu(LBF_2)$ and $Cu(TAAB)^+$ suggest that both complexes contain Cu(I).[14] Molecular orbital theory has also been employed to address the question of the oxidation state of copper in the formally Cu(I) complexes. The results of extended Hückel theory (EHT) calculations on $Cu(TIM)^+$, $Cu(LBF_2)$, and $Cu(TAAB)^+$ indicate that the first two complexes are best described as containing Cu(III) centers while $Cu(TAAB)^+$ contains a Cu(I) center.[17]

The SCF–Xα–SW method is much less approximate than simple HF–LCAO models and has provided excellent predictions for electronic and EPR spectra for a variety of complexes.[20,21] The Xα–SW method also provides information regarding the bonding system not available from EHT. Xα–SW calculations on two relevant macrocyclic systems, Fe(TIM)[22,23] and copper porphine,[20] have appeared in the literature. SCF–Xα–SW calculations were performed on models of $Cu(TIM)^{2+}$, $Cu(TIM)^+$, and $Cu(TIM)Cl^+$ (**2**, **3**) with

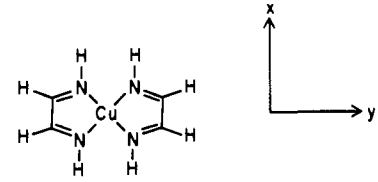

2

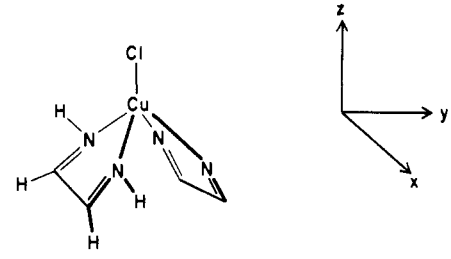

3

following goals: (i) determining the nature and relative energies of the molecular orbitals of primarily Cu 3d character in the four-coordinate planar complexes and in five-coordinate pyramidal complexes (this information could be helpful in understanding the changes that occur in the molecular orbitals upon addition of a fifth ligand and the role that these changes play in determining the "unusual" position of Cl^- in the spectrochemical series observed for Cu(TIM)L complexes and other pyramidal macrocyclic Cu complexes); (ii) providing insight into the ground-state electronic structure of the reduced cation $Cu(TIM)^+$ and the changes that occur in the molecular orbitals upon reduction; (iii) assigning the electronic transitions and interpreting the EPR spectra observed for the compounds; (iv) providing further evidence of the role played by PF_6^- in determining the solid-state properties of $[Cu(TIM)Cl]PF_6$.[9]

Computational Section

The Cu–N bond distances used to calculate $Cu(TIM)^{2+}$ and two models for $Cu(TIM)Cl^+$ were 1.945, 1.955 (solid-state model), and 1.988 (solution-state model) Å, respectively. Other bond lengths and angles are shown in supplementary Tables I and II. Those for $Cu(TIM)^{2+}$ were taken from the crystal structure of $[Cu(TIM)](BPh_4)_2$.[10] TIM was modeled by $N_2C_2H_4$, with N–H = 1.00 Å and C–H = 1.05 Å. Parameters for the "solid-state" $Cu(TIM)Cl^+$ model were obtained from the crystal structure of $[Cu(TIM)Cl]PF_6$,[10] where the anion is an important structural element. The "solution-state" model was designed to reflect the changes that might occur when the cation and anion are separated by solvation. These changes include the further displacement of the Cu atom from the N_4 plane and the shortening of the axial Cu–Cl bond. Data obtained from the crystal structure of $[Cu(TIM)(1\text{-MeIm})](PF_6)_2$[10,11] (see supplementary Tables I and II) were used to determine the positions of the two $N_2C_2H_4$ fragments and the Cu atom, which lies 0.09 Å farther out of the N_4 plane in this model than in the solid-state model. The apical Cl atom was positioned by maintaining the Cl–N contact distance at 3.35 Å. This new position results in the shortening of the Cu–Cl bond by 0.107 Å from that found in the $[Cu(TIM)Cl]PF_6$ structure. This positioning of the Cl is reasonable since one of the factors that appears to be important in the absence of steric effects in determining the axial M–Cl distance in pyramidal tetraaza macrocyclic complexes is repulsion between the axial Cl and N atoms. Examples of Cl–N contacts for pyramidal tetraaza macrocyclic complexes may be found in Table XII and range from 3.3 to 3.4 Å regardless of the degree of metal displacement from the N_4 plane.

The initial molecular potentials for $Cu(N_2C_2H_4)_2^{2+}$ and the "solid-state" model of $Cu(N_2C_2H_4)_2Cl^+$ were constructed by superposition of the atomic SCF–Xα charge densities. Overlapping sphere

(13) Gagné, R. R.; Allison, J. L.; Lisensky, G. C. *Inorg. Chem.* **1978**, *17*, 3563–3571.
(14) Gagné, R. R.; Allison, J. L.; Koval, C. A.; Mialki, W. S.; Smith, T. J.; Walton, R. A. *J. Am. Chem. Soc.* **1980**, *102*, 1905–1909.
(15) Katovic, V.; Taylor, L. T.; Urbach, F. L.; White, W. H.; Busch, D. H. *Inorg. Chem.* **1972**, *11*, 479–483.
(16) Takvoryan, N.; Farmery, K.; Katovic, V.; Lovecchio, F. V.; Gore, E. S.; Anderson, L. U.; Busch, D. H. *J. Am. Chem. Soc.* **1974**, *96*, 731–742.
(17) Burdett, J. K.; Williams, P. D. *Inorg. Chem.* **1980**, *19*, 2770–2784.
(18) Gagné, R. R.; Ingle, D. M. *J. Am. Chem. Soc.* **1980**, *102*, 1444–1446.
(19) Martin, J. W. L.; Timmons, J. H.; Martell, A. E.; Rudolf, P.; Clearfield, A. *Inorg. Chem.* **1981**, *20*, 814–821.
(20) Case, D. A.; Karplus, M. *J. Am. Chem. Soc.* **1977**, *99*, 6182–6194.
(21) (a) Case, D. A. *Annu. Rev. Phys. Chem.* **1982**, *33*, 151–171. (b) Johnson, K. H. *Ibid.* **1975**, *26*, 39–57.
(22) Norman, J. G., Jr.; Chen, L. M. L.; Perkins, C. M.; Rose, N. J. *Inorg. Chem.* **1981**, *20*, 1403–1409.
(23) Lawton, L. M. M.S. Thesis, University of Washington, 1979.

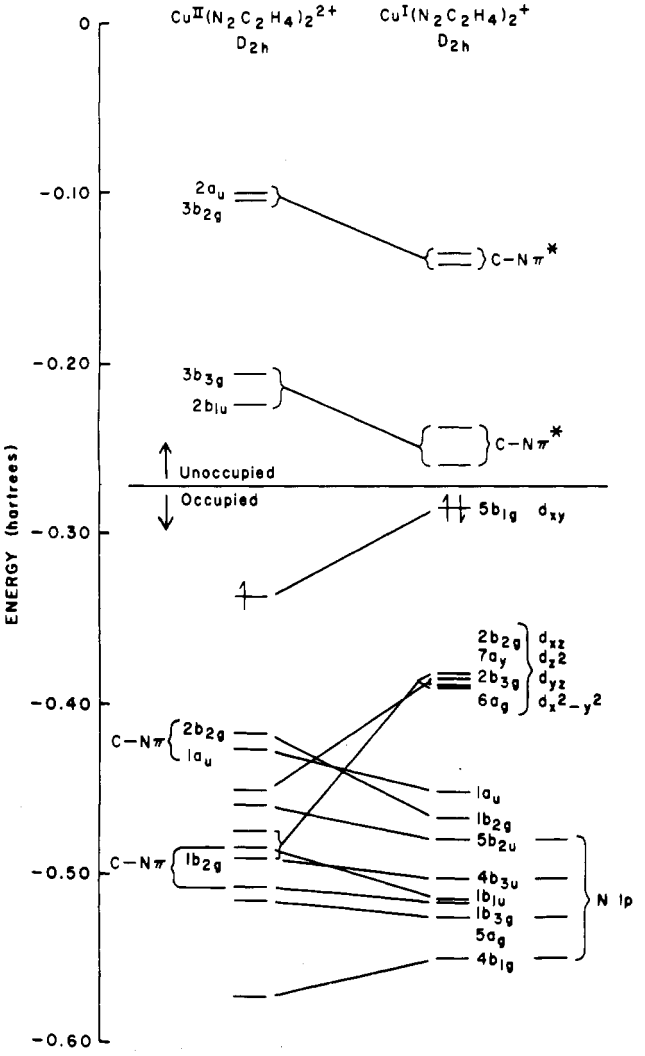

Figure 1. Frontier orbitals of $Cu(N_2C_2H_4)_2^{2+}$ and $Cu(N_2C_2H_4)_2^{+}$. The number of electrons in the highest occupied orbitals are shown. The Cu 3d or $N_2C_2H_4$ level with which an orbital most closely correlates is indicated.

radii (see supplementary Table III) were chosen by our nonempirical procedure as 88% of the atomic number radii.[24] The SCF calculations of $Cu(N_2C_2H_4)_2^{+}$ were initiated from the converged potential of $Cu(N_2C_2H_4)_2^{2+}$. The SCF calculation of the "solution-state" Cu(TIM)Cl^{+} model was started from the converged potential of the "solid-state" model. In both cases the sphere radii remained unchanged from those employed in the starting models. An additional calculation of $Cu(N_2C_2H_4)_2^{+}$ was also performed with use of precise 88% atomic radii (see supplementary Table III). In all cases, Watson spheres of opposite charge were employed to simulate lattice and solvation effects.[25]

The charge densities and potentials for all the complexes were corrected for double counting of charge in the sphere-overlap regions.[24,26,27] Any residual negative intersphere charge was set to zero, and the charge in the other regions was appropriately renormalized.

Spherical harmonics through $l = 4$, 2, 1, and 0 were used in the extramolecular, Cu, C and N, and H regions, respectively, to expand the wave function. Four possible configurations for $Cu(N_2C_2H_4)^{2+}$ were calculated to determine the one with the lowest total energy. Convergence of 0.0001 hartree was reached for all energy levels in the ground-state models.

The converged spin-restricted potentials for all four ground-state models were converted to spin-unrestricted potentials and reconverged.

(24) Norman, J. G., Jr. *Mol. Phys.* **1976**, *31*, 1191–1198.
(25) Watson, R. E. *Phys. Rev.* **1958**, *111*, 1108–1110.
(26) Herman, F. "Electrons in Finite and Infinite Structures"; Phariseau, P., Scheire, L., Eds.; Plenum Press: New York, 1977; pp 382–410.
(27) Yang, C. Y.; Johnson, K. H. *Int. J. Quantum Chem., Symp.* **1976**, *No. 10*, 159–165.

Table I. Distribution of Cu, Cl, and $N_2C_2H_4$ Spherical-Harmonic Basis Functions among Representations of D_{2h} and C_{2v}[a]

representations				
D_{2h}	C_{2v}	Cu	Cl	$(N_2C_2H_4)_2$[b]
a_g	a_1	s, d_{z^2}, $d_{x^2-y^2}$	s	$\sigma + \sigma$
b_{1g}	a_2	d_{xy}		$\pi^* + \pi^*$
b_{2g}	b_1	d_{xz}		$\sigma^* - \sigma^*$
b_{3g}	b_2	d_{yz}		$\pi - \pi$
a_u	a_2			$\pi^* - \pi^*$
b_{1u}	a_1	p_z	p_z	$\sigma - \sigma$
b_{2u}	b_2	p_y	p_y	$\pi + \pi$
b_{3u}	b_1	p_x	p_x	$\sigma^* + \sigma^*$

[a] The coordinate system used is shown in Figure 1. [b] The symbols σ and σ^* refer to in-plane orbitals of individual $N_2C_2H_4$ groups that are respectively symmetric and antisymmetric with respect to the C_2 axis. Similarly, π and π^* refer to the out-of-plane p-orbital combinations. There is no differentiation between orbitals that are C-N bonding and antibonding within individual $N_2C_2H_4$ groups.

Table II. Spin-Restricted Valence Energy Levels (E, hartrees)[a] and Charge Distribution[b] for $Cu(N_2C_2H_4)_2^{2+}$

		% charge[b]					Cu sphere			
D_{2h} level	$-E$	Cu	4 N	4 C	4 H_N	4 H_C	% d	% s	% p	type[c]
$4a_g$	0.6578	18	41	40	0	1	38	62	0	$4a_1$
$4b_{2u}$	0.6242	5	35	55	0	4				$4a_1$
$4b_{1g}$	0.5716	53	33	5	4	5	100	0	0	$4b_1$
$5a_g$	0.5149	36	14	36	5	10	87	13	0	$5a_1$
$1b_{3g}$	0.5065	57	29	15	0	0	100	0	0	$1b_2$
$1b_{2g}$	0.4896	87	11	2	0	0	100	0	0	d_{xz}
$4b_{3u}$	0.4895	13	71	5	7	4	0	0	100	$4b_1$
$1b_{1u}$	0.4842	1	60	39	0	0				$1b_2$
$6a_g$	0.4736	99	0	0	0	0	100	0	0	$d_{x^2-y^2}$
$5b_{2u}$	0.4590	11	45	27	7	10	0	0	100	$5a_1$
$7a_g$	0.4503	81	10	6	2	2	85	15	0	d_{z^2}
$2b_{3g}$	0.4500	59	21	21	0	0	100	0	0	d_{yz}
$1a_u$	0.4255	0	78	22	0	0				$1a_2$
$2b_{2g}$	0.4168	22	60	18	0	0	100	0	0	$1a_2$
$5b_{1g}$	0.3369	56	39	2	2	1	100	0	0	d_{xy}
$2b_{1u}$	0.2237	5	38	57	0	0				$2b_2$
$3b_{3g}$	0.2071	2	49	49	0	0				$2b_2$
$3b_{2g}$	0.1040	1	22	77	0	0				$2a_2$
$2a_u$	0.0996	0	26	74	0	0				$2a_2$

[a] All levels between −0.70 and −0.005 hartree except for diffuse Rydberg-state orbitals. Levels below −0.70 hartree are essentially ligand σ in character with <2% Cu character. [b] Relative amounts of charge within Cu, four α-diimine nitrogens, etc. spheres. [c] Cu or ligand orbital most closely corresponding to the orbital in question. See ref 22 for energy level diagram and characterization of the ligand orbitals.

These potentials were used to calculate hyperfine coupling constants by the method of Case and Karplus[20,28] and used as the starting point for calculating electronic transitions with use of the transition-state procedure.[29]

Results

The Cu and Cl atomic orbitals and the α-diimine fragment orbitals that may combine with each other are listed in Table I according to their representations in D_{2h} and C_{2v} symmetry.

The calculated upper valence levels and charge distributions for $Cu(N_2C_2H_4)_2^{2+}$, $Cu(N_2C_2H_4)_2^{+}$, and solid- and solution-state $Cu(N_2C_2H_4)_2Cl^{+}$ are listed in Tables II–V. Also shown in these tables is a correlation between the molecular orbitals and the ligand and metal orbitals from which they are derived.[22] The absolute energies of the molecular orbitals of $Cu(N_2C_2H_4)_2^{+}$ depicted in Figure 1 were made comparable

(28) Case, D. A.; Karplus, M. *Chem. Phys. Lett.* **1976**, *39*, 33–38.
(29) Slater, J. C. "Quantum Theory of Molecules and Solids"; McGraw-Hill: New York, 1974; Vol. 4.

Table III. Spin-Restricted Valence Energy Levels (E, hartrees) and Charge Distribution for $[Cu(N_2C_2H_4)_2]^{+}$ [a]

D_{2h} level	$-E$	% charge Cu	4 N	4 C	4 H_N	4 H_C	Cu sphere % d	% s	% p	type
$4a_g$	0.5905	11	37	49	0	2	26	74	0	$4a_1$
$4b_{2u}$	0.5660	3	32	60	1	4	100	0	0	$4a_1$
$4b_{1g}$	0.4686	38	50	4	5	3	100	0	0	$4b_1$
$5a_g$	0.4444	19	29	33	8	10	41	59	0	$5a_1$
$1b_{3g}$	0.4356	9	53	39	0	0	100	0	0	$1b_2$
$1b_{1u}$	0.4335	1	56	43	0	0				$1b_2$
$4b_{3u}$	0.4218	11	73	5	7	3	0	0	100	$4b_1$
$5b_{2u}$	0.3983	11	51	22	7	9	0	0	100	$5a_1$
$1b_{2g}$	0.3861	18	64	18	0	0	100	0	0	$1a_2$
$1a_u$	0.3701	0	76	24	0	0				$1a_2$
$6a_g$	0.3098	99	0	0	0	0	100	0	0	$d_{x^2-y^2}$
$2b_{3g}$	0.3083	94	0	6	0	0	100	0	0	d_{yz}
$7a_g$	0.3046	98	1	0	1	0	94	6	0	d_{z^2}
$2b_{2g}$	0.3012	88	7	5	0	0	100	0	0	d_{xz}
$5b_{1g}$	0.2051	72	25	2	1	0	100	0	0	d_{xy}
$2b_{1u}$	0.1804	5	41	54	0	0				$2b_2$
$3b_{3g}$	0.1588	5	52	42	0	0				$2b_2$
$3b_{2g}$	0.0637	2	21	77	0	0				$2a_2$
$2a_u$	0.0577	0	29	71	0	0				$2a_2$

[a] For definitions and explanations of table categories, see the footnotes to Table II.

to those of $Cu(N_2C_2H_4)_2^{2+}$ by setting the energy of the $1a_g$ orbital of the former model equal to the energy of the $1a_g$ orbital of the latter model and adjusting the remaining orbitals accordingly. This procedure, which is designed to account for the differences in the energies of the orbitals caused by different molecular charges and Watson spheres used, is reasonable because the $1a_g$ orbital is a ligand orbital that is not expected to vary significantly in absolute energy in different models.

Table VI summarizes the estimated atomic charges. These were obtained by partitioning the extramolecular and intersphere charges among the atomic spheres according to the relative charges on the sphere surfaces and then taking the difference between the number of valence electrons so calculated and the number found in the neutral atom.[28]

Discussion

$Cu(N_2C_2H_4)_2^{2+}$. The SCF-Xα-SW molecular orbital diagram for $Cu(N_2C_2H_4)_2^{2+}$ (Figure 1) is very similar to that for $Fe(N_2C_2H_4)_2(NCS)_2^{0,+}$.[22] The major differences involve the relative ordering of the mainly metal 3d and ligand π orbitals. In the iron complexes, the three occupied and two unoccupied 3d-like orbitals are above the C–N π orbitals, with the unoccupied pair overlapping the also-unoccupied C–N π^* orbitals. In the copper(II) complex, the four fully occupied 3d-like orbitals overlap the C–N π band, with the singly occupied $3d_{xy}$-like orbital ($5b_{1g}$) above, but still well below the C–N π^* orbitals. The lowering of d-like relative to ligand-like orbitals is expected in passing from iron to more electronegative copper.

The agreement between the theoretically predicted and experimentally observed[9] electronic spectra (see Table VII) provides evidence that the predicted ordering and relative energies of the frontier orbitals of $Cu(N_2C_2H_4)_2^{2+}$ accurately reflect the ground state of $[Cu(TIM)](BPh_4)_2$. The observed absorptions at 3.85 and 2.94 μm^{-1} may be assigned to LMCT bands: $5b_{2u} \rightarrow 5b_{1g}$ and $1a_u \rightarrow 5b_{1g}$, respectively. These transitions arise from orbitals on the ligand that are nitrogen lone pair and C–N π in character.

The energy of the observed shoulder (2.3 μm^{-1}) lies between the energies predicted for two symmetry-forbidden transitions: $7a_g \rightarrow 5b_{1g}$ (2.57 μm^{-1}) and $2b_{2g} \rightarrow 5b_{1g}$ (1.99 μm^{-1}). $7a_g \rightarrow 5b_{1g}$ can be described as a d–d transition. The change in Cu character and the relaxation energy exhibited by the $2b_{2g} \rightarrow 5b_{1g}$ transition are intermediate between the values expected for a LMCT transition and a d–d transition (see Table VII); thus, neither label clearly applies. The assignment of the observed shoulder to the $2b_{2g} \rightarrow 5b_{1g}$ transition is somewhat ambiguous but consistent with the assignment of the $5b_{2u} \rightarrow 5b_{1g}$ and $1a_u \rightarrow 5b_{1g}$ transitions, which are predicted to occur at energies somewhat lower than actually observed. Further, this assignment is consistent with the assignment of the lowest energy transition for $Cu(N_2C_2H_4)_2Cl^+$, which involves the analogous orbitals.

The EPR spectrum of $Cu(N_2C_2H_4)_2^{2+}$ was calculated by using the conventional perturbation approach developed for square-planar Cu complexes.[30] The relevant molecular orbitals in D_{4h} symmetry can be expressed in the form

$$b_{1g} = \alpha d_{xy} - \tfrac{1}{2}\alpha'[-\sigma_1 x + \sigma_2 y + \sigma_3 x - \sigma_4 y]$$

$$b_{2g} = \beta d_{x^2-y^2} - \tfrac{1}{2}\beta'[\pi_1 y + \pi_2 x - \pi_3 y - \pi_4 x]$$

$$e_g = \delta d_{xz} - (\delta/2^{1/2})[\pi_a z - \pi_b z]$$

$$e_g = \delta d_{xz} - \delta/2^{1/2}[\pi_2 z - \pi_4 z]$$

The model exhibits D_{2h} symmetry, like that found for the donor atoms of $[Cu(TIM)](BPh_4)_2$. The latter complex displays an EPR spectrum indistinguishable from an axial one with use of an X-band spectrometer.[9] The deviation from D_{4h} symmetry is therefore perceived to be small, and the spectrum is interpreted with use of D_{4h} expressions. The EPR spectrum was interpreted in terms of the spin Hamiltonian

$$H = \beta_e \vec{H}\cdot\mathbf{g}\cdot S + I_{Cu}\cdot\mathbf{A}_{Cu}\cdot S + I_N\cdot\mathbf{A}_N\cdot S$$

where $\vec{H}$ is the external field, $\mathbf{g}$ is the effective g tensor, β_e is the Bohr magneton, S is the electron spin, I_{Cu} and I_N are nuclear spins, and $\mathbf{A}_{Cu}$ and $\mathbf{A}_N$ are nuclear hyperfine tensors. The quadrupole couplings for Cu and N are neglected. The $\mathbf{g}$, $\mathbf{A}_{Cu}$, and $\mathbf{A}_N$ tensors depend on the wave functions of the system and have been calculated by using the following equations and the results from both spin-restricted and spin-unrestricted wave functions. The expressions used for evaluating the $\mathbf{g}$ tensor were

$$g_\parallel = 2.0023 - \frac{8\lambda\alpha^2\beta^2}{\Delta(b_{2g} \rightarrow b_{1g})}$$

$$g_\perp = 2.0023 - \frac{2\lambda\alpha^2\delta^2}{\Delta(e_g \rightarrow b_{1g})}$$

where the ligand contribution is assumed to be negligible in analogy with studies on copper porphine.[20] The expressions used for the components of the hyperfine tensors were

$$A_\parallel = P\left[-\tfrac{4}{7}\alpha^2 - K - 2\lambda\alpha^2\left(\frac{4\beta^2}{\Delta(b_{2g} \rightarrow b_{1g})} + \frac{3\delta^2}{7\Delta(e_g \rightarrow b_{1g})}\right)\right]$$

$$A_\perp = P\left[\tfrac{2}{7}\alpha^2 - K - \frac{11\lambda\alpha^2\delta^2}{7\Delta(e_g \rightarrow b_{1g})}\right]$$

In these expressions α and δ are coefficients defined above, λ is the spin–orbit coupling constant for the free ion (−828 cm^{-1} for Cu(II)), $P = \beta_e g_e \beta_N g_N \langle r^{-3}\rangle_{3d}$ (0.0388 cm^{-1} for $^{63}Cu(II)$[31]), and K is the contact term, which has been found to vary from 0.30 to 0.35 for a variety of copper compounds.[32] An average

(30) Kuska, H. A.; Rogers, M. T. "Spectroscopy in Inorganic Chemistry"; Academic Press: New York, 1971; Vol. 2, p 175.
(31) McGarvey, B. R. *J. Phys. Chem.* **1967**, *71*, 51–67.

Table IV. Spin-Restricted Valence Energy Levels (E, hartrees) and Charge Distribution for Solid-State $Cu(N_2C_2H_4)_2Cl^{+}$ [a]

C_{2v} level	$-E$	% charge						Cu sphere			type
		Cu	4 N	4 C	4 H_N	4 H_C	Cl	% d	% s	% p	
$5a_1$	0.6314	14	40	44	0	2	0	36	63	2	$4a_1$
$4b_2$	0.6036	5	35	56	0	4	0				$4a_1$
$4a_2$	0.5415	55	33	4	4	4	0	100	0	0	$4b_1$
$6a_1$	0.4981	36	18	32	5	9	0	86	14	0	$5a_1$
$4b_1$	0.4866	54	38	3	3	2	0	92	0	8	d_{xz}
$5b_2$	0.4863	55	26	17	1	1	0	100	0	0	d_{yz}
$7a_1$	0.4692	7	54	37	1	1	0				$1b_2$
$6b_2$	0.4531	15	44	30	4	6	0	64	0	36	$5a_1$
$8a_1$	0.4528	96	1	0	0	0	3	99	1	0	d_{x^2}
$5b_1$	0.4453	44	46	4	3	2	1	86	14	0	$4b_1$
$9a_1$	0.4381	71	9	6	2	1	10	89	11	0	$d_{y^2-z^2}$
$7b_2$	0.4189	51	27	16	3	3	1	91	0	9	$1b_2$
$5a_2$	0.4031	0	78	22	0	0	0				$1a_2$
$6b_1$	0.3956	24	59	17	0	0	0	99	0	1	$1a_2$
$6a_2$	0.3195	54	41	2	2	1	0	100	0	0	d_{xy}
$10a_1$	0.3064	16	4	4	0	0	76	67	2	32	$3p_z$
$7b_1$	0.3030	1	1	0	0	0	98				$3p_x$
$8b_2$	0.3027	1	1	0	0	0	98				$3p_y$
$11a_1$	0.2057	3	44	49	0	0	5				$2b_2$
$9b_2$	0.1965	2	51	47	0	0	0				$2b_2$
$8b_1$	0.0880	1	22	77	0	0	0				$2a_2$
$7a_2$	0.0834	0	26	74	0	0	0				$2a_2$

[a] For definitions and explanations of table categories, see the footnotes to Table II.

value of 0.325 was used for K. In D_{2h} symmetry, the e_g levels are not degenerate. This gives rise to the equations

$$g_{\parallel} = g_{zz} = 2.0023 - \frac{8\lambda\alpha^2\beta^2}{\Delta_1}$$

$$g_{xx} = 2.0023 - 2\lambda\alpha^2\left(\frac{\delta_1^2}{\Delta_2} + \frac{\delta_3^2}{\Delta_4}\right)$$

$$g_{yy} = 2.0023 - 2\lambda\alpha^2\left(\frac{\delta_2^2}{\Delta_3} + \frac{\delta_4^2}{\Delta_5}\right)$$

$$g_{\perp} = \frac{g_{xx} + g_{yy}}{2}$$

$$A_{\parallel} = A_{zz} = P\left\{\frac{-4\alpha^2}{7} - K - 2\lambda\alpha^2\left[\frac{4\beta^2}{\Delta_1} + \frac{3}{14}\left(\frac{\delta_1^2}{\Delta_2} + \frac{\delta_2^2}{\Delta_3} + \frac{\delta_3^2}{\Delta_4} + \frac{\delta_4^2}{\Delta_5}\right)\right]\right\}$$

$$A_{xx} = P\left[\frac{2\alpha^2}{7} - K - \frac{11\lambda\alpha^2}{7}\left(\frac{\delta_1^2}{\Delta_2} + \frac{\delta_3^2}{\Delta_4}\right)\right]$$

$$A_{yy} = P\left[\frac{2\alpha^2}{7} - K - \frac{11\lambda\alpha^2}{7}\left(\frac{\delta_2^2}{\Delta_3} + \frac{\delta_4^2}{\Delta_5}\right)\right]$$

$$A_{\perp} = \frac{A_{xx} + A_{yy}}{2}$$

where the parameters of α^2, β^2, δ^2, and Δ are defined in Table IX. The results, shown in Table X, are in good agreement with those obtained from powder spectra of $[Cu(TIM)](BPh_4)_2$.[9]

Use of spin-unrestricted wave functions allows the Fermi contact coupling arising from spin polarization to be evaluated directly. Spin-unrestricted wave functions were also employed to obtain values for the contact term and direct dipolar terms. The spin–orbit contribution was evaluated from the spin-restricted wave functions. These values are also shown in Table X. The value calculated for the Fermi contact contribution (-0.0098 cm^{-1}) is much smaller than the value of $-PK$ (-0.0126 cm^{-1}) and leads to values for $A_{\parallel}$ and $A_{\perp}$ with greater discrepancy from experiment than those when the semiempirical value, $-PK$, is used. This observation is in agreement with that made in the Xα–SW treatment of the copper porphine EPR spectrum.[20]

Also shown in Table X are values for the nitrogen hyperfine coupling constants obtained from the spin-unrestricted wave functions. The values obtained from the calculations are in good agreement with experiment.[9] A triumph of the calculations is that $^{N}A_{\parallel}$ is predicted to be less than $^{N}A_{\perp}$, as experimentally found. In the calculation of copper porphine, the opposite situation is predicted ($^{N}A_{\parallel} > {}^{N}A_{\perp}$) and found experimentally.[33]

The order of the Cu 3d orbitals in the crystal field sense is found to be $d_{xy} > d_{z^2} > d_{x^2-y^2} > d_{xz}, d_{yz}$ when the average energies of the molecular orbitals with significant amounts of d_{xz} and d_{yz} character are used to determine the positions of the d_{xz} and d_{yz} orbitals in the series. This order is different than that predicted for four-coordinate planar Cu(II) complexes on the basis of polarized spectra and EPR studies of Cu(II) bis(β-ketoenolates).[34] This difference reflects the σ-donor ability of the α-diimine fragments and the lack of any significant π interaction between the Cu d_{xz}, d_{yz} orbitals and the TIM π* system. The energy difference between the d_{xy} and d_{z^2} orbitals predicted for $[Cu(TIM)](BPh_4)_2$ is 2.49 μm^{-1}, which is in excellent agreement with estimates of the in-plane ligand field strength of TIM obtained from studies of six-coordinate, low spin $Fe(TIM)^{2+}$ [35] and $Co(TIM)^{3+}$ [7] complexes (2.4–2.6 μm^{-1}).

$Cu(N_2C_2H_4)_2^{+}$. The calculated ground state of this ion (^1A_g), in which the mainly Cu $3d_{xy}$ orbital ($5b_{1g}$) now has two electrons, is best described as containing Cu(I). The ground state has a total energy 11 000 cm^{-1} below the $^1A_u(Cu^{II}(N_4^-))$ excited state and 33 000 cm^{-1} below the ^1A_g $(Cu^{III}(N_4^{2-}))$

(32) Maki, A. H.; McGarvey, B. R. *J. Chem. Phys.* **1958**, *29*, 31–38.

(33) Manoharan, P. T.; Rogers, M. T. "Electron Spin Resonance of Metal Complexes"; Yeh, T. F., Ed.; Adam Hilger: New York, 1969; p 143.
(34) Cotton, F. A.; Wise, J. J. *Inorg. Chem.* **1967**, *6*, 917–924.
(35) Dabrowiak, J. C.; Merrell, P. H.; Stone, J. A.; Busch, D. H. *J. Am. Chem. Soc.* **1973**, *95*, 6613–6622.

Table V. Spin-Restricted Valence Energy Levels (E, hartrees) and Charge Distribution for Solution-State $Cu(N_2C_2H_4)_2Cl^+$ [a]

C_{2v} level	$-E$	% charge						Cu sphere			type
		Cu	4 N	4 C	4 H_N	4 H_C	Cl	% d	% s	% p	
$5a_1$	0.6234	11	37	49	0	3	0	32	65	2	$4a_1$
$4b_2$	0.6005	4	32	58	1	5	0				$4a_1$
$4a_2$	0.5258	57	32	4	3	3	0	100	0	0	$4b_1$
$6a_1$	0.4855	45	19	25	4	7	0	92	8	0	$5a_1$
$4b_1$	0.4823	56	35	3	3	2	0	94	0	6	d_{xz}
$5b_2$	0.4792	53	27	18	0	1	1	100	0	0	d_{yz}
$7a_1$	0.4663	7	52	37	2	2	0				$1b_2$
$8a_1$	0.4493	88	2	2	0	1	8	97	3	0	d_{x^2}
$6b_2$	0.4464	28	38	28	3	4	0	89	0	11	$5a_1$
$9a_1$	0.4382	70	9	7	2	1	12	90	10	0	$d_{y^2-z^2}$
$5b_1$	0.4354	38	50	5	3	2	2	84	0	16	$4b_1$
$7b_2$	0.4069	40	35	15	4	4	2	85		5	$1b_2$
$5a_2$	0.4024	0	78	22	0	0	0				$1a_2$
$6b_1$	0.3959	27	57	16	0	0	0	98	0	2	$1a_2$
$6a_2$	0.3221	52	43	2	2	1	0	100	0	0	d_{xy}
$10a_1$	0.3112	22	5	4	0	0	69	66	2	29	$3p_z$
$7b_1$	0.3053	3	1	0	0	0	96				$3p_x$
$8b_2$	0.3048	3	1	0	0	0	96				$3p_y$
$11a_1$	0.1984	2	45	50	0	0	3				$2b_2$
$9b_2$	0.1901	1	51	47	0	0	0				$2b_2$
$8b_1$	0.0819	1	22	77	0	0	0				$2a_2$
$7a_2$	0.0765	0	26	74	0	0	0				$2a_2$

[a] For definitions and explanations of table categories, see the footnotes to Table II.

Table VI. Estimated Atomic Charges[a] for $Cu(N_2C_2H_4)_2^{2+,+}$ and $Cu(N_2C_2H_4)_2Cl^+$

	$Cu(N_2C_2H_4)_2^{2+}$ $^2B_{1g}$	$Cu(N_2C_2H_4)_2^{+}$ [b] ^1A_g	$Cu(N_2C_2H_4)_2Cl^+$ $^2A_2$	
			solid state	soln state
Cu	0.07+	0.34−	0.04+	0.03+
N	0.17−	0.20−	0.18−	0.18−
C	0.34+	0.26+	0.32+	0.32+
H_N	0.23+	0.20+	0.20+	0.21+
H_C	0.09+	0.07+	0.07+	0.06+
Cl			0.71−	0.66−

[a] See text for method of estimation. [b] Model with precise 88% atomic radii.

Table VII. Electronic Spectra of $Cu(N_2C_2H_4)_2^{2+}$ and $Cu(N_2C_2H_4)_2^{+}$ [a]

complex	D_{2h} transition[b]	D_{2h} excited state	Δ(% Cu)$_{gs}$[c]	energy, calcd	energy, exptl[d]
$Cu(N_2C_2H_4)_2^{2+}$	$2b_{2g} \rightarrow 5b_{1g}$	$^2B_{2g}$	33	1.99	2.3 (sh)
	$7a_g \rightarrow 5b_{1g}$	^2A_g	−26	2.57	
	$1a_u \rightarrow 5b_{1g}$	^2A_u	57	2.79	2.94
	$5b_{2u} \rightarrow 5b_{1g}$	$^2B_{2u}$	46	3.47	3.85
$Cu(N_2C_2H_4)_2^{+}$	$5b_{1g} \rightarrow 2b_{1u}$	^1A_u	−60	1.33	1.34

[a] All energies in μm^{-1}. [b] Only spin-allowed transitions are listed. [c] Difference between copper character of the upper and lower orbitals of the transition in the ground state. [d] See ref 9.

Table VIII. Electronic Spectra of Solid- and Solution-State $Cu(N_2C_2H_4)_2Cl^+$ [a]

model	C_{2v} transition	C_{2v} excited state	Δ(% Cu)$_{gs}$	energy, calcd	energy, exptl
solid state	$6b_1 \rightarrow 6a_2$	$^2B_1$	27	1.87	1.68
	$7b_2 \rightarrow 6a_2$	$^2B_2$	−1	2.25	
	$5a_2 \rightarrow 6a_2$	$^2A_2$	55	2.59	
solution state	$6b_1 \rightarrow 6a_2$	$^2B_1$	23	1.77	1.53
	$7b_2 \rightarrow 6a_2$	$^2B_2$	9	1.96	2.15
	$5a_2 \rightarrow 6a_2$	$^2A_2$	50	2.44	

[a] For definitions and explanations of table categories, see the footnotes to Table VII.

excited state. That the oxidation-state change represents an increase in the actual negative charge on the Cu center is substantiated by the atomic charges calculated for Cu in each model (see Table VI). The formally Cu(I) complexes of TIM, LBF_2, and TAAB are characterized by intense absorptions at 1.34,[36] 1.48,[37] and 1.42[16] μm^{-1}, respectively. For $Cu(TIM)^+$ this transition is assigned to the MLCT transition ($^1A_g \rightarrow {}^1A_u$) calculated to occur at 1.33 μm^{-1} in the theoretical model (see Table VII).

Table IX. Parameters Used in Calculating EPR Results from the Spin-Restricted Wave Functions of $Cu(N_2C_2H_4)_2^{2+}$

orbital	Cu coeff	$10^4\Delta$, cm^{-1}
$5b_{1g}$	α^2, 0.56	
$6a_g$	β^2, 0.99	3.00
$2b_{2g}$	δ_1^2, 0.22	0.88
$2b_{3g}$	δ_2^2, 0.59	2.48
$1b_{2g}$	δ_3^2, 0.87	3.35
$1b_{3g}$	δ_4^2, 0.57	3.72

The comparison of molecular orbital diagrams for $Cu(N_2C_2H_4)_2^+$ and $Cu(N_2C_2H_4)_2^{2+}$ (Figure 1) illustrates the changes that occur upon reduction of the Cu(II) complex. The Cu 3d orbitals are raised in energy and no longer mix extensively with the ligand orbitals, behaving essentially as nonbonding orbitals. The lower lying $4a_g$ and $5a_g$ orbitals contain significantly larger amounts of Cu s character in the Cu(I) complex. The orbitals with contributions from Cu p functions ($4b_{3u}$, $5b_{2u}$) are essentially unchanged.

Although no significant metal–ligand π interaction is found in either $Cu(N_2C_2H_4)_2^{2+}$ or $Cu(N_2C_2H_4)_2^+$, transfer of elec-

(36) Addison, A. W.; Carpenter, M.; Lau, L. K.-M.; Wicholas, M. *Inorg. Chem.* **1978**, *17*, 1545–1552.
(37) Gagné, R. R.; Allison, J. L.; Gall, R. S.; Koval, C. A. *J. Am. Chem. Soc.* **1977**, *99*, 7170–7178.

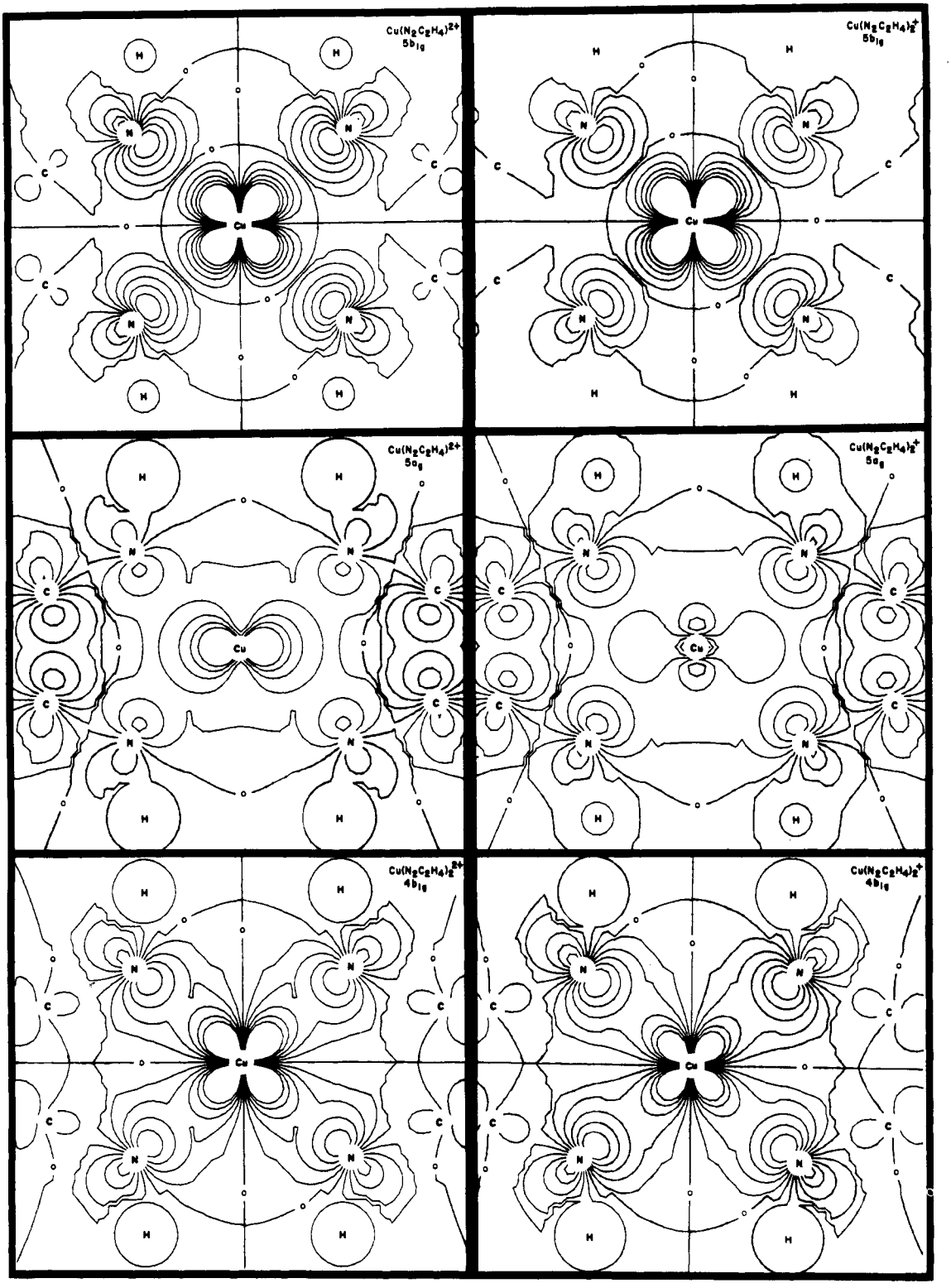

Figure 2. Contour maps of the molecular wave functions of $Cu(N_2C_2H_4)_2^{2+}$ and $Cu(N_2C_2H_4)_2^{+}$ in the *xy* plane showing the σ interactions between Cu and the ligands. The $5b_{1g}$ orbital gains 0.88 electron upon reduction. The $5a_g$ orbital is the orbital involved in metal to ligand back-donation in the σ system and is antibonding with respect to the imine C–N σ bond. The contour values in this and subsequent maps are 0, 0.04, 0.08, 0.12, 0.16, and 0.20 (electron/a_0^3)$^{1/2}$. The zero contours are labeled to indicate changes of sign in the wave functions.

tron density from metal to ligand does occur upon reduction in the σ *system* (a_g and b_{1g} orbitals). Tables II and III show that 88% of the electron added to the $5b_{1g}$ orbital ends up on the Cu center. Table VI, however, shows that the total negative charge on Cu increases by only 0.41 electron. Thus, the ligand receives the majority of the new electron density (0.59 electron). While 0.12 electron comes from the electron added to $5b_{1g}$, a larger amount comes from a shift of density from Cu to the ligand in $4,5a_g$ (0.48 electron) and $4b_{1g}$ (0.30 electron). In $7a_g$, 0.34 electron is shifted from ligand to Cu, so that the net increase in ligand population in the σ system is 0.56 electron, 95% of the total increase of 0.59 electron.

The ligand C=N stretching frequency in Cu(II) α-diimine complexes is observed to decrease upon one-electron reduction.[13] Close examination of orbital contour maps, as exemplified by Figure 2, shows that, while the $4b_{1g}$ and $5b_{1g}$ orbitals are largely C–N nonbonding, certain of the a_g orbitals (for example, $5a_g$) are significantly C–N antibonding. The transfer

Table X. EPR Results for $Cu(N_2C_2H_4)_2^{2+}$ [a]

	Xα-SW	exptl[b]		Xα-SW	exptl[b]
		Spin Restricted			
$g_\parallel$	2.124	2.141	$A_\parallel$	−0.0196	−0.0216
g_{xx}	2.050		A_{xx}	−0.0050	
g_{yy}	2.039		A_{yy}	−0.0053	
$g_\perp$	2.044	2.037	$A_\perp$	−0.0052	≅−0.0040
		Spin Unrestricted			
		Cu			
a[c]	−0.0098 (−0.0126)[e]		A_{yy}^{so}	0.0011	
$A_\parallel^{dd}$	−0.0144		$A_\parallel^{f}$	−0.0216[g]	−0.0216
A_{xx}^{d}	0.0047		A_{xx}^{f}	−0.0065	
A_{yy}^{d}	0.0073		A_{yy}^{f}	−0.0042	
$A_\parallel^{so}$	0.0054		$A_\perp$	−0.0054	−0.0040
A_{xx}^{so}	0.0014				
		N			
a	0.0017		$A_\parallel$	0.0015	
$A_\parallel^{d}$	−0.0002		A_{xx}	0.0015	
A_{xx}^{d}	−0.0002		A_{yy}	0.0021	0.0012
A_{yy}^{d}	0.0004		$A_\perp$	0.0018	0.0015

[a] All hyperfine coupling constants in cm^{-1}. [b] See ref 9. The signs of $A_\parallel$ and $A_\perp$ are assumed to be consistent with theory. [c] Contact term. [d] Dipolar contact term. [e] Semiempirical contact term = $-PK$. [f] Sum of contact, dipolar, and spin-orbit terms. [g] Calculated with $a = -0.0126$ cm^{-1} (see text).

of σ electron density from Cu to ligand in these orbitals upon reduction may be responsible for the observed decrease in $\nu_{C\equiv N}$.

$Cu(N_2C_2H_4)Cl^+$. The factors influencing the character of metal d orbitals in square-pyramidal complexes have been investigated semiquantitatively with use of EHT,[38,39] and qualitative applications of the results have been made to interpret the bonding in Cu(MeTIM)L complexes.[40] The effect of mixing 4s and 4p orbital character into the metal $3d_{z^2}$ orbital was shown to minimize the antibonding interaction between this orbital (filled for Cu(II)) and the apical ligand, while maximizing π bonding with p_z symmetry orbitals of the equatorial ligands as the metal is moved out of the basal ligand plane.[38,39] These favorable interactions were shown to be offset to a degree by the loss of π bonding between the metal d_{xz} and d_{yz} orbitals and ligand p_z symmetry orbitals as the metal is displaced from the equatorial ligand plane.[38,39] In addition, antibonding interactions between the d_{xz}, d_{yz} orbitals and all ligands was suggested to be minimized by mixing $4p_{x,y}$ character into these orbitals.[38,39] Because the Cu 3d orbitals are nearly filled, it has been suggested that the 4s and 4p orbitals might be expected to be important in interpreting the bonding interactions in pyramidal Cu(MeTIM)L complexes.[40]

The addition of a fifth ligand to $Cu(N_2C_2H_4)_2^{2+}$ has only subtle effects on the interaction between copper and the α-diimine units. The molecular orbital diagram for the "solid-state" $Cu(N_2C_2H_4)_2Cl^+$ (Figure 3) illustrates the relative positions of the singly occupied orbital ($6a_2$) and three orbitals that are mostly ligand in character. The last three orbitals occur between the $6a_2$ and the next Cu 3d orbital. Two of these orbitals ($6b_1$ and $7b_2$) have significant amounts of metal character. The displacement of the Cu from the plane of the macrocycle alters the interaction between the metal d_{xz} and d_{yz} orbitals and the nitrogen p_z orbitals of TIM from essentially nonbonding to weak σ and σ* interactions. This is illustrated

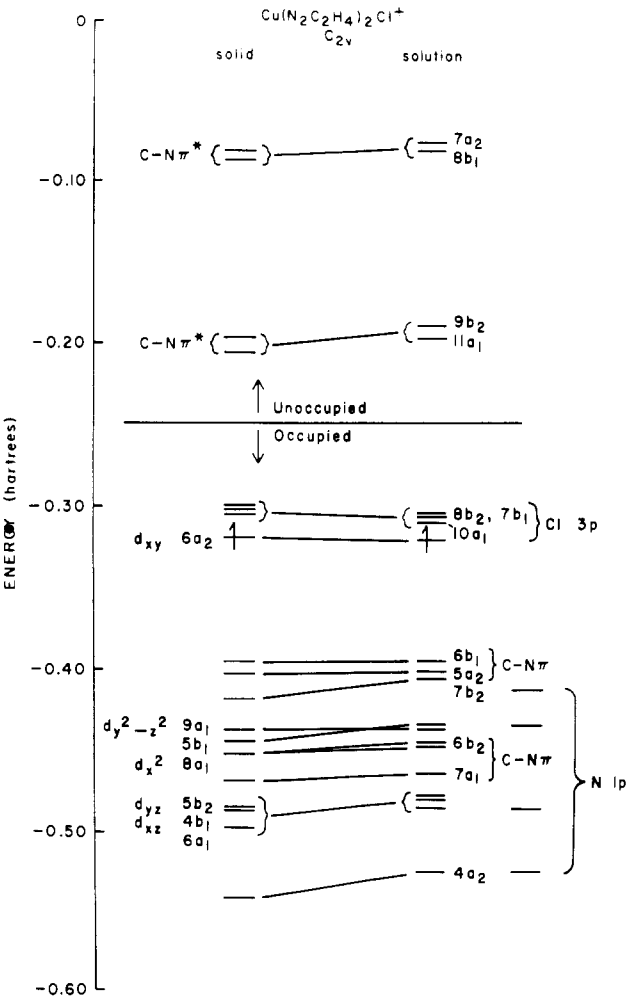

Figure 3. Frontier orbitals of solid-state and solution-state $Cu(N_2C_2H_4)_2Cl^+$. The HOMO's, LUMO's and the orbitals containing the unpaired electrons are shown for both models. The Cu 3d, $N_2C_2H_4$, or Cl 3p orbital with which each orbital most closely correlates is indicated.

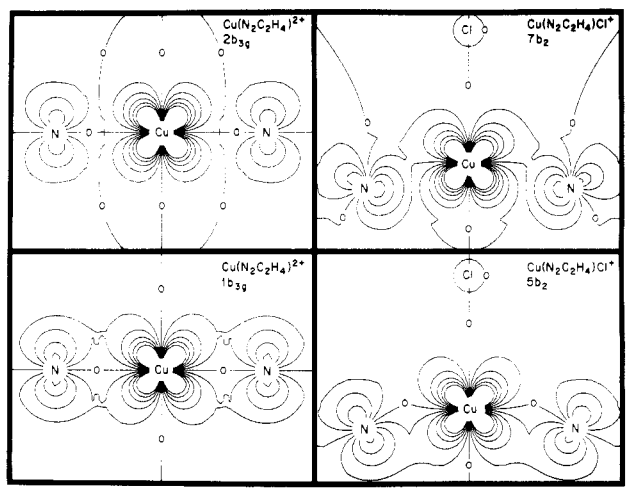

Figure 4. Contour maps of the molecular wave functions of $Cu(N_2C_2H_4)_2^{2+}$ and solid-state $Cu(N_2C_2H_4)_2Cl^+$ in a plane perpendicular to the *xy* plane containing two Cu–N bonds. The orbitals shown are the ones to which the d_{yz} orbital contributes.

(38) Rossi, A. R.; Hoffmann, R. *Inorg. Chem.* **1975**, *14*, 365–374.
(39) Elian, M.; Hoffmann, R. *Inorg. Chem.* **1975**, *14*, 1058–1076.
(40) Coltrain, B. K.; Jackels, S. C. *Inorg. Chem.* **1981**, *20*, 2032–2039.
(41) Reuveni, A.; Malatesta, V.; McGarvey, B. R. *Can. J. Chem.* **1977**, *55*, 70–75.
(42) Caira, E. B.; Nassibeni, L. R.; Wooley, P. R. *Acta Crystallogr., Sect. B: Struct. Crystallogr. Cryst. Chem.* **1975**, *B31*, 1334–1338.
(43) Weiss, M. C.; Bursten, B.; Peng, S. M.; Goedken, V. L. *J. Am. Chem. Soc.* **1976**, *98*, 8021–8031.
(44) Hoard, J. L.; Cohen, G. H.; Glick, M. D. *J. Am. Chem. Soc.* **1967**, *89*, 1992–1996.
(45) Koenig, D. F. *Acta Crystallorgr.* **1965**, *18*, 663–673.
(46) Sletten, E. *Acta Crystallogr., Sect. B: Struct. Crystallogr. Cryst. Chem.* **1970**, *B26*, 1609–1614.

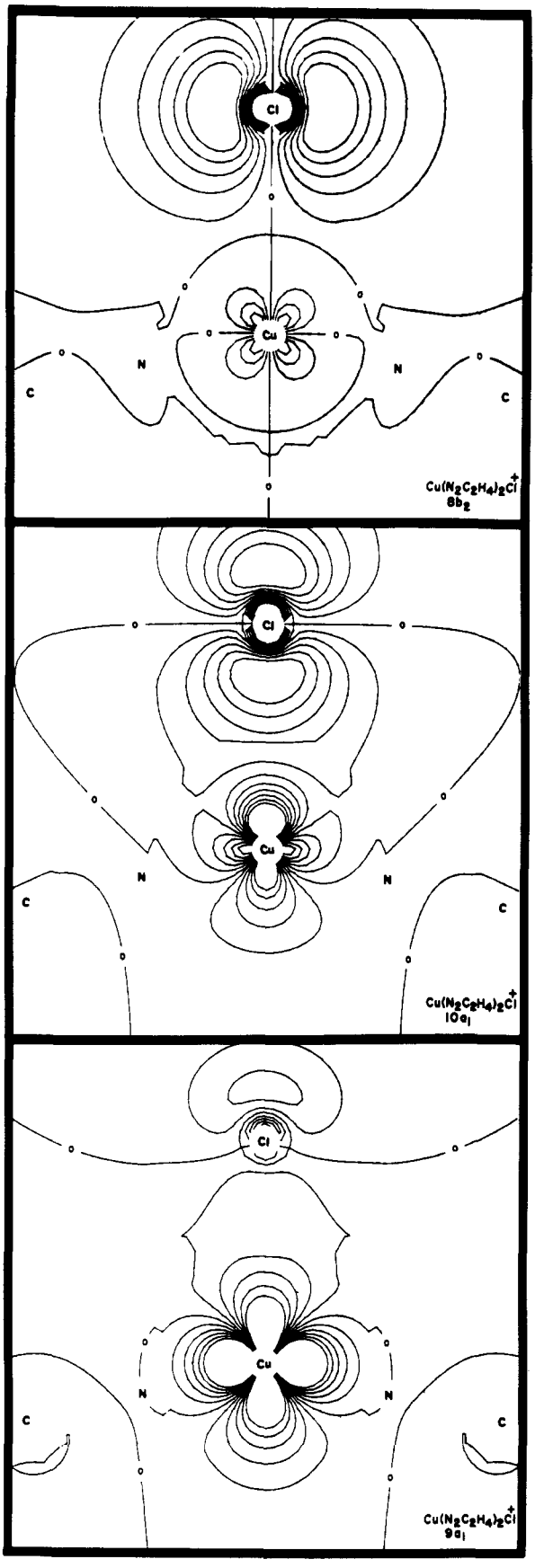

Figure 5. Contour maps of the molecular wave function of solid-state $Cu(N_2C_2H_4)_2Cl^+$ in the *yz* plane illustrating the interaction between Cu and Cl.

for the molecular orbitals to which the d_{yz} orbital contributes in $Cu(N_2C_2H_4)_2^{2+}$ and $Cu(N_2C_2H_4)_2Cl^+$ in Figure 4. The last two orbitals show the expected effect of mixing with the

Table XI. Spin Unrestricted EPR Results for the Solution-State $Cu(N_2C_2H_4)_2Cl^+$ Model[a]

	Xα-SW	exptl[b]		Xα-SW	exptl[b]
		Cu			
a	−0.0058 (−0.126)		A_{yy}^{so}	0.0010	
$A_{\parallel}^{d}$	−0.0131		$A_{\parallel}$	0.0206	−0.0195
A_{xx}^{d}	−0.0065		A_{xx}	0.0055	
A_{yy}^{d}	−0.0066		A_{yy}	0.0056	
A^{so}	−0.0051		$A_{\perp}$	−0.0056	−0.0030
A_{xx}^{so}	0.0010				
		N			
a	0.0017		$A_{\parallel}$	0.0016	
$A_{\parallel}^{d}$	−0.0001		A_{xx}	0.0015	
A_{xx}^{d}	−0.0002		A_{yy}	0.0023	
A_{yy}^{d}	−0.0006		$A_{\perp}$	−0.0019	
		Cl			
a	0.0001		A_{yy}	−0.0000	
$A_{\parallel}$	−0.0001	0.0051[c]	$A_{\perp}$	−0.0000	
A_{xx}	−0.0000				

[a] All values in cm^{-1}; all terms defined in Table X. [b] See ref 9. [c] Obtained from spectral simulation.

$4p_y$ orbital,[38,39] although only to a small extent (see Table IV).

The results of the calculations indicate that the antibonding interactions between the Cu and Cl atoms in $Cu(TIM)Cl^+$ can be minimized without mixing large amounts of 4p character to the Cu 3d orbitals of a_1 symmetry. These orbitals are the d_{x^2} ($8a_1$) and $d_{y^2-z^2}$ ($9a_1$) orbitals, which contain no Cu 4p character. The observed reorientation of the 3d orbitals with respect to the molecular coordinate system upon addition of an axial Cl^- ligand minimizes the antibonding interactions between the metal and the ligands.

The interaction between the Cu(II) center and the axial chloride ion in $[Cu(TIM)Cl]PF_6$ is predicted to be mainly ionic. There is some covalent σ interaction between the copper and the chloride in the $9a_1$ and $10a_1$ orbitals (Table IV). The Cu–Cl π interaction is essentially zero. The nature of the Cu–Cl interaction in this compound is depicted by the wave function contour diagrams in Figure 5. The small amount of covalency in the Cu–Cl bond results in the placement of three filled orbitals, which are nearly pure Cl 3p orbitals, above the singly occupied $6a_2$ orbital. Thus, the HOMO ($8b_2$) in the ground state of this complex is a Cl 3p orbital. The high negative charge found on Cl (Table VI) is another indication of the substantial ionicity of the bond.

The lowest energy electronic transition for the solid-state $Cu(N_2C_2H_4)_2Cl^+$ model is the $6b_1 \rightarrow 6a_2$ transition. This transition involves orbitals analogous to those involved in the $2b_{2g} \rightarrow 5b_{1g}$ transitions of $Cu(N_2C_2H_4)_2^{2+}$. As was the case for the planar model, the orbital relaxation and difference in Cu character computed for the $6b_1 \rightarrow 6a_2$ transition are not consistent with either a LMCT (i.e., $5a_2 \rightarrow 6a_2$) or a d–d (i.e., $7b_2 \rightarrow 6a_2$) transition (see Table V). In C_{2v} symmetry this transition is symmetry allowed. The broad, low-energy transition observed for $[Cu(TIM)Cl]PF_6$ is tentatively assigned to the $6b_1 \rightarrow 6a_2$ transition on the basis of the agreement between the calculated and experimental energies (see Table VIII).

A crystal field interpretation of the lowest energy transition would fail to describe the nature of the $6b_1$ orbital, which is mostly ligand in character in the ground state. It is apparent that the low-energy transition cannot be described as an envelope of d–d transitions from the results of these calculations. This conclusion is in agreement with the fact that no multiplicity has been observed in this transition.[9] However, more spectroscopic studies are needed to confidently assign the broad low-energy absorption in the spectrum of $[Cu(TIM)Cl]PF_6$ to a single transition.

Table XII. Cl-N Contact Distances

complex	av M-N, Å	av M-Cl, Å	av Cl-M-N, deg	σ, Å[a]	Cl-N contact dist, Å[b]	ref
$[Cu(Me_2(N\text{-}Me)[15]trieneN_4)Cl]NO_3$	1.97	2.50	99.8	0.34	3.44	42
$[Fe(C_{22}H_{22}N_4)Cl]\cdot CH_3CN$	2.00	2.25	107.3	0.60	3.43	43
[Fe(TPP)Cl]	2.05	2.19	100.7	0.38	3.27	44
[Fe(proto-IX)Cl]	2.06	2.22	103.7	0.48	3.37	45
$[Cu(purine)_2Cl]$[c]	2.00	2.43	98.3	0.29	3.36	46
$[Cu(TIM)Cl]PF_6$	1.96	2.40	100.1	0.33	3.35	10

[a] Metal displacement from N_4 plane. [b] Sum of van der Waals radii for Cl and N is 3.3 Å. [c] Not a macrocyclic structure.

The solution-state $Cu(N_2C_2H_4)_2Cl^+$ model was designed to explore the influence of the amount of Cu displacement from the N_4 plane of the macrocycle and of the axial ligand–Cu bond shortening on the electronic spectrum of the complex. This in turn would test the hypothesis that the PF_6^- anion present in $[Cu(TIM)Cl]PF_6$ influences the electronic spectrum of the solid by holding the Cu atom closer to the N_4 plane of the macrocycle through electrostatic interactions.

The electronic spectrum calculated for the solution-state model (Table VIII) features a red shift in the $6b_1 \rightarrow 6a_2$ transition of 0.10 μm^{-1} from that calculated for the solid-state model. Comparisons of the results of calculations on the solid- and solution-state models (see Tables IV and V) allow an explanation for the experimentally observed red shift in the spectrum of $[Cu(TIM)Cl]PF_6$ (0.14 μm^{-1})[9] to be advanced. The shortening of the Cu–Cl bond by 0.107 Å in the solution-state model increases covalency in the bond only slightly. Further, it has essentially no effect on the energy of the $d_{y^2-z^2}$ orbital. Since the Cu–N distance was the same in the two models, the Cu displacement would seem to be the main factor involved in determining the energy of the lowest energy electronic transition in this complex.

The energy of the $7b_2 \rightarrow 6a_2$ transition (the lowest energy d–d transition) is also red shifted from that calculated for the solid-state model (see Table VIII). However, this transition is still predicted to occur at much higher energy than the $6b_1 \rightarrow 6a_2$ transition.

Insights concerning the important factors involved in determining the EPR spectrum of $[Cu(TIM)Cl]PF_6$ can be gained through analysis of the calculated EPR parameters for the solution-state model. The values of $g_\parallel$, $g_\perp$, $A_\parallel$, and $A_\perp$ may be evaluated in a manner similar to that employed for $Cu(N_2C_2H_4)_2^{2+}$. All orbitals of a_1 symmetry contribute to $g_\parallel$, and all orbitals of b_1 and b_2 symmetry will contribute to g_{xx} and g_{yy}, respectively. The formulas used for computing the g values are

$$g_{zz} = g_\parallel = 2.0023 - 8\lambda\alpha^2\sum_{n=1}^{n}\frac{\beta_n^2}{\Delta_n}$$

$$g_{xx,yy} = 2.0023 - 2\lambda\alpha^2\sum_{x=1}^{x}\frac{\delta x^2}{\Delta_x}$$

where all symbols have the meanings defined previously.

When $g_\parallel$ is calculated by using the spin-restricted wave functions with contributions from the $5–9a_1$ orbitals, a value of 2.167 is obtained. This value is in excellent agreement with the experimental value of 2.165. The values of g_{xx} and g_{yy} were both calculated to be 2.04 and are also in good agreement with the experimental value of 2.06. (The contributing orbitals were $4–7b_1$ for g_{xx} and $5–8b_2$ for g_{yy}.)

The contributions to A_{zz}, A_{xx}, and A_{yy} arising from the Fermi contact term and the dipolar terms were calculated from the spin-unrestricted wave functions and appear in Table XI. The calculated Fermi contact term is again much smaller than the semiempirical value. If the empirical value is used, then the sum of the direct contact, dipolar, and spin–orbit terms leads to a value of -0.0206 cm^{-1} for $A_\parallel$. This value is in reasonable agreement with the experimental value of -0.0195 cm^{-1}. The value for $A_\perp$ contained in Table XI was obtained similarly.

These data support the observed trend for g values to increase and A values to decrease upon addition of a fifth ligand. This trend should continue with increasing displacement of the Cu since, as previously noted, the main effect of displacing the Cu is the lowering of the $6a_2$ orbital. This would decrease the energy difference between the $6a_2$ and the a_1, b_1, and b_2 symmetry orbitals that lie below it and in turn result in positive shifts in the g values and to decreases in the absolute values of $A_\parallel$, $A_\perp$, and A_{iso}.

The hyperfine coupling constants that describe the interaction of the unpaired spin with nitrogen and chlorine nuclei were estimated via spectral simulation with use of the method of Reuveni et al.[4]

The value predicted by the spin-unrestricted Xα–SW model for $^{Cl}A_\parallel$ is not large enough to account for the features in the experimentally observed spectrum ($^{Cl}A_\parallel \cong 0.0051$ cm^{-1}).[9] The reasons for this underestimate are not clear. However, the model used in the calculations may not accurately reflect the nature of the Cu–Cl interaction in CH_2Cl_2 solution at 100 K, the conditions under which the spectrum was obtained.[9]

Acknowledgment. This research was supported by grants for J.G.N. from the NSF and the Petroleum Research Fund, administered by the American Chemical Society. We thank Professor Norman J. Rose for advice and Professor David A. Case for helpful discussions and a critical review of the manuscript.

Supplementary Material Available: Listings of bond lengths and angles used in the Xα–SW calculations and atomic and outer-sphere radii (3 pages). Ordering information is given on any current masthead page.